

FIRST INTRINSIC ANISOTROPY OBSERVATIONS WITH THE COSMIC BACKGROUND IMAGER

S. PADIN, J. K. CARTWRIGHT, B. S. MASON, T. J. PEARSON, A. C. S. READHEAD,
M. C. SHEPHERD, J. SIEVERS, AND P. S. UDOMPRASERT

California Institute of Technology, 1200 East California Boulevard, Pasadena, CA 91125

W. L. HOLZAPFEL

University of California, 426 LeConte Hall, Berkeley, CA 94720-7300

S. T. MYERS

National Radio Astronomy Observatory, P.O. Box O, Socorro, NM 87801

J. E. CARLSTROM AND E. M. LEITCH

University of Chicago, 5640 South Ellis Ave., Chicago, IL 60637

M. JOY

Dept. of Space Science, SD50, NASA Marshall Space Flight Center, Huntsville, AL 35812

AND

L. BRONFMAN AND J. MAY

Departamento de Astronomía, Universidad de Chile, Casilla 36-D, Santiago, Chile

Draft version October 25, 2018

ABSTRACT

We present the first results of observations of the intrinsic anisotropy of the cosmic microwave background radiation with the Cosmic Background Imager from a site at 5080 m altitude in northern Chile. Our observations show a sharp decrease in C_l in the range $l = 400$ – 1500 . The broadband amplitudes we have measured are $\delta T_{\text{band}} = 58.7^{+7.7}_{-6.3} \mu\text{K}$ for $l = 603^{+180}_{-166}$ and $\delta T_{\text{band}} = 29.7^{+4.8}_{-4.2} \mu\text{K}$ for $l = 1190^{+261}_{-224}$, where these are half-power widths in l . Such a decrease in power at high l is one of the fundamental predictions of the standard cosmological model, and these are the first observations which cover a broad enough l range to show this decrease in a single experiment. The C_l we have measured enables us to place limits on the density parameter, $\Omega_{\text{tot}} \leq 0.4$ or $\Omega_{\text{tot}} \geq 0.7$ (90% confidence).

Subject headings: cosmic microwave background — cosmology: observations

1. INTRODUCTION

In standard cosmologies, spatial temperature variations in the cosmic microwave background radiation (CMBR) are closely related to the primordial density fluctuations which gave rise to the formation of all structure in the universe (Peebles & Yu 1970; Sunyaev & Zeldovich 1970). The angular power spectrum of these temperature variations on the celestial sphere, C_l , yields a direct estimate of the prime cosmological parameters and provides a fundamental link between particle physics and cosmology (e.g., Kamionkowski & Kosowsky 1999). Since radio interferometers sample the angular power spectrum directly and are straightforward to calibrate, they provide a simple and direct determination of C_l . Here we report the first observations of the CMBR with the Cosmic Background Imager (CBI).

2. THE COSMIC BACKGROUND IMAGER

The CBI is a radio interferometer with 13 0.9 m diameter antennas mounted on a 6 m tracking platform. It operates in 10 1 GHz frequency channels from 26 to 36 GHz. The instantaneous field of view and the maximum resolution are $\sim 45'$ and $\sim 3'$ (FWHM). The instrument has an altitude-azimuth mount, and the antenna platform can also be rotated about the optical axis to increase the aperture-plane (u, v) coverage and to facilitate polarization observations. The antennas have low-noise broadband high-electron mobility transistor (HEMT) amplifier receivers with ~ 25 K noise temperatures. The typical system noise temperature averaged over all 10 bands is ~ 30 K, in-

cluding ground spillover and atmosphere. The frequency of operation of the CBI was chosen as a compromise between the effects of astronomical foregrounds, atmospheric emission, and the sensitivity that can be achieved with HEMT amplifiers. Details of the instrument design may be found in Padin et al. (2000a,b, S. Padin et al. 2000, in preparation) and on the CBI web site.¹ The CBI is located at an altitude of 5080 m near Cerro Chajnantor in the Atacama desert in northern Chile. This site was chosen because the atmospheric opacity is low and the CBI can operate at the thermal noise limit much of the time. The instrument was assembled and tested on the Caltech campus during 1998 and 1999 and shipped to Chile in 1999 August. Installation of the telescope and site infrastructure were completed by the end of 1999, and the full instrument has been in operation since early 2000 January.

The CBI is sensitive to multipoles in the range $400 < l < 4250$, where these values reflect the half-power widths of the window functions on the shortest and longest baselines. The CBI complements BOOMERANG (de Bernardis et al. 2000; Lange et al. 2001), the Degree Angular Scale Interferometer (DASI) (Halverson et al. 1998), *Microwave Anisotropy Probe*,² MAXIMA (Hanany et al. 2000; Balbi et al. 2000), and the Very Small Array (Jones & Scott 1998), which cover the range $50 < l < 1000$. DASI is a sister project to the CBI, and the CBI and DASI designs were chosen to complement each other. The CBI control software and correlator and receiver control electronics were duplicated by the DASI team for the DASI project. Together these two interferometers cover the multipole range

¹ See <http://www.astro.caltech.edu/~tjp/CBI>.

² See the *MAP* Web site at <http://map.gsfc.nasa.gov/>.

$100 < l < 4250$.

3. OBSERVATIONS

The antenna platform of the CBI permits a wide variety of antenna configurations. For observations during the test phase (2000 January–April) we chose a configuration with the antennas around the perimeter of the platform, which provided easy access to the receivers and fairly uniform (u, v) coverage, enabling us to test the full range of CBI baselines. We report here only observations on baselines corresponding to $l < 1510$, which account for 25% of the data in this ring configuration. We do not report on the higher multipole bins because these are more dependent on the bright-source and statistical faint-source corrections, which are still preliminary. These results, and mosaicked observations which significantly increase the resolution in l , will be presented elsewhere.

We based our flux density scale on observations of Jupiter, assuming $T_{\text{Jupiter}} = 152$ K at 32 GHz, with 5% uncertainty (Mason et al. 1999). The spectral index of Jupiter is not constant between 26 and 36 GHz (Wrixon et al. 1971), so we used Taurus A as our prime calibrator. Taurus A is slightly resolved with the CBI, but it can be well fitted by an elliptical Gaussian model. We referenced the 32 GHz flux density of Taurus A to that of Jupiter and transferred this to the other frequency channels assuming $\alpha_{\text{Taurus A}} = -0.30$, where $S \propto \nu^\alpha$ (Mezger et al. 1986). Any uncertainties resulting from this extrapolation are $< 1\%$.

For our intrinsic anisotropy observations, we selected regions at Galactic latitudes above 20° , for which the synchrotron emission and the IRAS 100 μm emission are relatively low, and which avoided bright point sources detected in the NRAO Very Large Array 1.4 GHz Sky Survey (NVSS) (Condon et al. 1998). These regions are also in the declination range $-5^\circ < \delta < -2^\circ$, which permits point-source monitoring with the Owens Valley Radio Observatory (OVRO) 40 m telescope (see § 5).

Daytime observations of the CMBR are not possible because radio emission from the Sun contaminates the visibilities. Radio emission from the Moon causes similar problems, and intrinsic anisotropy observations are restricted to fields more than 60° from the moon. The weather during 2000 January–April was uncommonly poor, and we lost 50% of the nights as a result of bad weather. In the remaining nights the observing conditions were superb, and the sensitivity was limited by the system noise.

The dominant systematic contamination in the CBI observations is due to ground spillover. The level of contamination on the 1 m baselines is typically between a few tens and a few hundreds of mJy; in rare instances it can be as high as a few Jy, and it falls off with increasing baseline length. The ground signals can be recognized in the maps because they are not confined to the primary beam area, as celestial signals are. We have successfully removed the ground signal by differencing visibilities measured on two fields at the same declination separated by 08^{m} in right ascension. The observations were alternated between two fields on an 8 minute timescale, so that both fields were observed at the same position relative to the ground. In addition to filtering out ground spillover, this differencing strongly rejects crosstalk and other spurious instrumental signals. As discussed below, any residual spurious signals amount to $\lesssim 1.3\%$ of $C_l^{1/2}$ and may therefore safely be ignored. The differenced observations reported here are between two fields centered at $08^{\text{h}} 44^{\text{m}} 40^{\text{s}}$, $-03^\circ 10'$ and $08^{\text{h}} 52^{\text{m}} 40^{\text{s}}$, $-03^\circ 10'$; and

two fields centered at $14^{\text{h}} 42^{\text{m}}$, $-03^\circ 50'$ and $14^{\text{h}} 50^{\text{m}}$, $-03^\circ 50'$ (J2000). To search for residual spurious signals in excess of the thermal noise level in our differenced visibilities, we needed an accurate estimate of the thermal noise level. We obtained this estimate by computing the rms of successive 8.4 s integrations in the differenced visibilities. The typical noise level computed in this way was 2 Jy, in agreement with the (less accurate) noise level determined from the system temperature. The means of the 8^{m} scans were much smaller than 2 Jy, so this method provided an accurate estimate of the thermal noise level. To test for residual spurious signals, we divided our differenced visibilities into two parts in three ways: (1) pre- versus posttransit observations; (2) middle half versus outer quarters of hour-angle range; and (3) first versus second half of epochs on each field (pre-March 23 vs. post-March 23).

In each case, we subtracted the singly differenced visibilities point by point in the (u, v) plane. In cases 1 and 2 the doubly differenced visibilities were consistent with the expected noise. In case 3 there was an excess amounting to a 1.3% contamination in $C_l^{1/2}$.

4. ANALYSIS AND RESULTS

We observed for 58.5 hr on each of the 08^{h} fields and for 16.15 hr on each of the 14^{h} fields. The sky signal is clearly visible in the differenced images on the 100 and 104 cm baselines (Fig. 1).

The extraction of the angular spectrum from visibility measurements is straightforward (White et al. 1999). The covariance matrix of the observations is the matrix of the covariances between all the visibility measurements:

$$C = M + N, \quad (1)$$

where M and N are the sky and noise covariance matrices. We assume that the noise on different baselines and at different frequencies is uncorrelated, i.e., that N is diagonal. The sky covariance matrix is

$$M_{jk} = \langle V(\mathbf{u}_j, \nu_j) V^*(\mathbf{u}_k, \nu_k) \rangle \quad (2)$$

$$= \int \int d^2\mathbf{v} \tilde{A}(\mathbf{u}_j - \mathbf{v}, \nu_j) \tilde{A}^*(\mathbf{u}_k - \mathbf{v}, \nu_k) S(\mathbf{v}, \nu_j, \nu_k) \quad (3)$$

for two visibility points j, k , where $\tilde{A}(\mathbf{u}, \nu)$ is the Fourier transform of the primary beam at frequency ν , \mathbf{u} is the baseline vector in wavelengths, and $S(\mathbf{v}, \nu_j, \nu_k)$ is a generalized power spectrum of the intensity fluctuations (Hobson et al. 1995). The effective weighting of this power spectrum defines the window function. The indices, j and k , run from 1 to n where n is the number of distinct (u, v) points. We average all the data taken at different times for each (u, v) point before doing the maximum likelihood calculation.

The generalized power spectrum is related to C_l by

$$S(\nu, \nu_j, \nu_k) = \left(\frac{2kT_0}{c^2} \right)^2 \nu_j^2 \nu_k^2 g(\nu_j) g(\nu_k) C_l, \quad (4)$$

where $l + \frac{1}{2} = 2\pi|\mathbf{v}|$ and the g factor is a small correction for the difference between the Rayleigh-Jeans and Planck functions. We can test a hypothetical power spectrum, $[C_l]$, by forming the likelihood function

$$L([C_l]) = \frac{1}{\pi^n \det C} \exp\{-V^*(\mathbf{u}_j) C_{jk}^{-1} V(\mathbf{u}_k)\}. \quad (5)$$

The cross-correlation between the signals received from two fields separated by 08^{m} in R.A. is negligible, so the expected

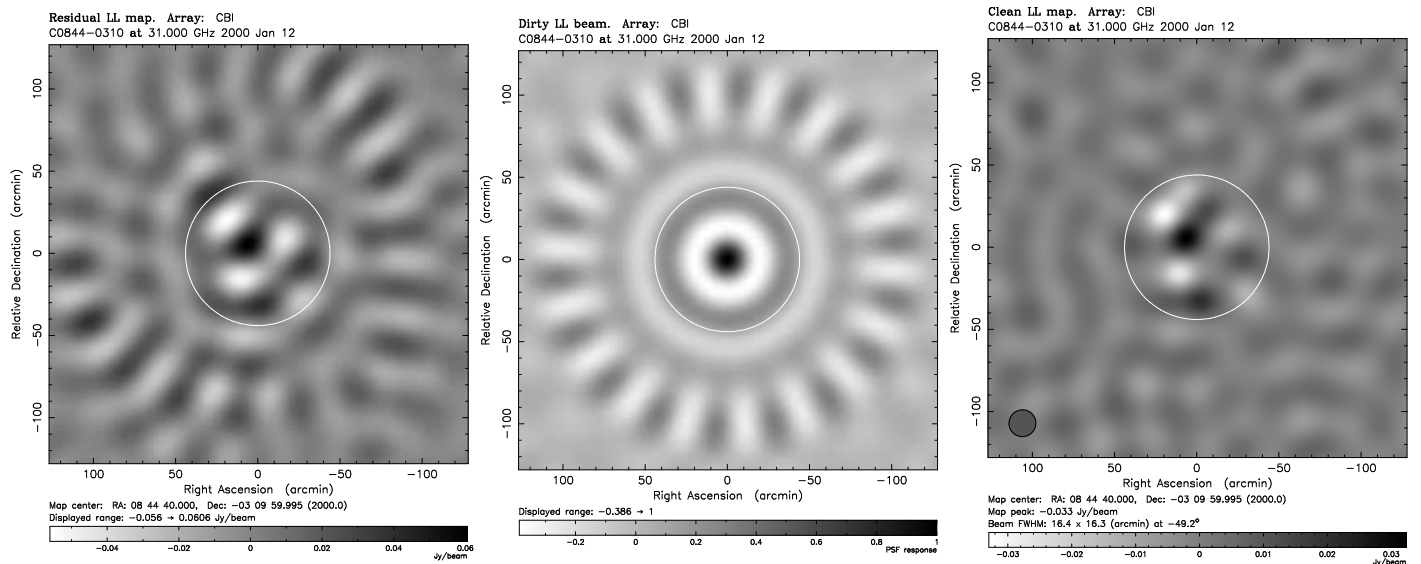


FIG. 1.— Differenced image of the 08^h field observed on the nine 100 cm and 104 cm CBI baselines in the test configuration (*left*), the corresponding point-spread function (*center*), and an image deconvolved with the Högbom CLEAN algorithm (*right*), assuming that the emission is confined to the primary-beam area. The 10 frequency channels have been combined, and the synthesized beamwidth $\sim 16'$ (FWHM). The circle at radius $44'$ indicates the primary-beam area which was cleaned. The structures outside the circle in the uncleared image (*left*) are due to sidelobes. These structures disappear after cleaning within the primary-beam area, indicating that they are caused by sidelobes.

variance of the differenced visibilities is twice the variance of the undifferenced visibilities. Our parametric model for C_l consists of two parameters, these being the amplitudes of C_l in the two ranges $l < 900$ and $l > 900$, assuming $l(l+1)C_l$ is constant in each range. In the test configuration there is a gap in our (u, v) coverage between $l = 800$ and $l = 1000$ which makes this a natural division. The band-power window functions, here approximated by sums of the single-baseline single-channel window functions within each l bin, may be characterized by $l = 603_{-166}^{+180}$ and $l = 1190_{-224}^{+261}$ (half-power widths). The maximum likelihood broadband signals we measure are $\delta T_{\text{band}} \equiv [l(l+1)C_l/(2\pi)]^{1/2} \times T_{\text{cmb}} = 58.7_{-6.3}^{+7.7} \mu\text{K}$ for the $l = 603$ bin and $\delta T_{\text{band}} = 29.7_{-4.2}^{+4.8} \mu\text{K}$ for the $l = 1190$ bin. The error bars indicate the points at which the likelihood has dropped by $e^{-0.5}$ (which are within 10% of the 68% integrated probability values). The results for the two fields, shown in Figure 2, agree to within the uncertainties. For the lower l bin, the uncertainties are dominated by sample variance, and they would be decreased by $< 2\%$ in the absence of thermal noise. For the upper l bin, the uncertainties would be decreased by 31% and 54% for the 08^h and 14^h fields, respectively, in the absence of thermal noise.

Our maximum likelihood analysis has been tested using software written independently by two of the authors, with no common code between the packages and using significantly different implementations for important steps, such as evaluation of the window function, binning and maximization algorithm. We have analyzed both the real data and simulated differenced data sets generated by realizations of known power spectra together with realistic noise and point sources. The results from these two software packages are in excellent agreement, and the simulations recover the original input power spectra. We have also generated 54 simulations of differenced sky images based on our observed band powers in the two bins (Fig. 2) and compared the rms signal, measured within the primary-beam area in these simulations, with the rms fluctuations in the primary beam measured in actual observations of 54 differenced fields, to be published elsewhere. Both the means and the distribu-

tions of the rms values for the observed and simulated fields are in excellent agreement. Thus, we are confident that our derived spectrum is a reliable representation of the signal that we have detected on the sky.

5. FOREGROUNDS

Radio galaxies and radio-loud quasars are a source of confusion at CBI frequencies and angular scales, so we equipped the OVRO 40 m telescope with a four-channel 26–34 GHz receiver for point-source monitoring, and observed all of the sources in the NVSS with $S_{1.4\text{GHz}} > 6$ mJy in our CBI fields. Those sources detected with the 40 m telescope at the 3σ level ($S_{30\text{GHz}} \geq 6$ mJy) have been subtracted from our CBI visibility data using the flux densities measured on the 40 m telescope. This reduced the levels of δT_{band} measured in the lower and upper l bins by 0.5% and 1%. We have also applied corrections based on the source count statistics (White et al. 1997) to account for point sources with $S_{30\text{GHz}} < 6$ mJy, which have not been subtracted individually from our visibility data. The corrections amounted to decreases in δT_{band} of 1.6% and 8.3% in the lower and upper l bins. These corrections have been applied to the band powers given in § 4. The uncertainty in the statistical correction, $\sim 20\%$, makes $\ll 0.1$ K difference to the errors in both bins.

It is unlikely that diffuse Galactic foreground emission is a significant contaminant in our observations. The expected rms fluctuations due to Galactic synchrotron emission on angular scales $5'–30'$ are $< 9 \mu\text{K}$ (e.g., Tegmark et al. 2000). In the RING5M experiment, Leitch et al. (1997) detected Galactic emission at 14.5 and 32 GHz with a spectrum consistent with free-free radiation but a much higher level than predicted from H α measurements. We have therefore made 14.5 GHz observations with the OVRO 40 m telescope along a strip at declination -5° over the right ascension range $0^{\text{h}}–24^{\text{h}}$. The beam and beamthrow, 7.4 and 22.2 , are fairly well matched to the CBI angular scales in the lower l bin, so, after correcting for the window function, we may use these observations to esti-

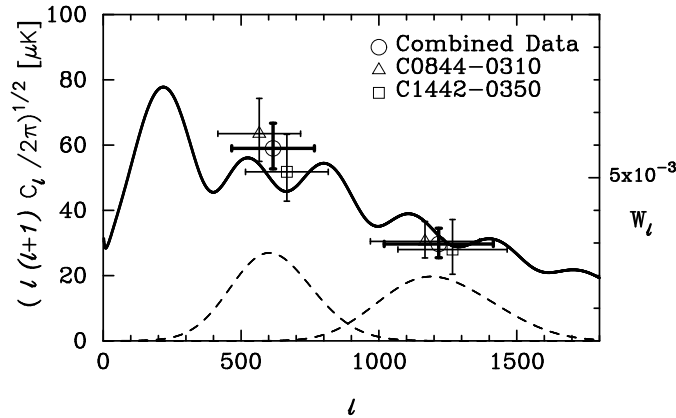


FIG. 2.— CMBR anisotropy spectrum determined from CBI observations. The triangles and squares show results on the 08^h and 14^h differenced fields; the circles show the results of a joint maximum likelihood analysis of both differenced fields. The individual 08^h and 14^h field results are offset in l for clarity. The window functions for each bin are shown as dashed lines. The solid curve represents a flat model universe with $H_0 = 75 \text{ km s}^{-1} \text{ Mpc}^{-1}$, $\Omega_b h^2 = 0.019$, and $\Omega_{\text{cdm}} = 0.2$.

mate the possible level of contamination in our CBI observations. If all of the signal seen at 14.5 GHz at $|b^{\text{II}}| > 5^\circ$ is attributed to anomalous emission with the same spectral properties as seen in the RING5m data, then this amounts to a component in our CBI observations $\delta T_{\text{band}} = 20 \mu\text{K}$ due to anomalous foregrounds. Subtraction in quadrature from the signal we have detected in the first l bin would reduce our observed δT_{band} by 7%.

We have measured the temperature spectral index, $\beta = \ln(T_1/T_2)/\ln(\nu_1/\nu_2)$, with 1 month of data from the CBI in a more compact configuration, optimized to measure both the angular spectrum and the radio-frequency spectrum of the CMBR. We find that the signal is primarily CMBR and not Galactic. We used a maximum likelihood analysis with β as a free parameter to determine that $\beta = 0.0 \pm 0.4$ (1σ error) in the lower l bin. If as much as 21% of the δT_{band} in this l bin were due to a free-free foreground component with spectral index $\beta = -2.1$, while the remainder was CMBR with $\beta = 0$, the spectral index measured would be < -0.8 , which is ruled out at the 2σ level. A 15% synchrotron foreground component with spectral index $\beta = -2.7$ can be ruled out at the same level.

6. DISCUSSION

A decrease in C_l at high l , caused by photon diffusion and the thickness of the last scattering region, is a fundamental prediction of the standard cosmological model (Silk 1968), and this is the first time that such a decrease has been detected in a single experiment. It is also the first time that anisotropy has been detected at $l > 1000$. The levels of δT_{band} detected with the CBI are consistent with observations at high l made over the last 12 years (Readhead et al. 1989; Scott et al. 1996; Church et al. 1997; Baker et al. 1999; Leitch et al. 2000; Holzapfel et al. 2000; Subrahmanyam et al. 2000). The level of δT_{band} we measure at $l \sim 600$ is a factor 1.5 higher than that found by BOOMERANG and a factor 1.3 higher than that found by MAXIMA; here we have used the best fit spectrum to the BOOMERANG+MAXIMA+DMR data (Jaffe et al. 2001) to extrapolate the BOOMERANG and MAXIMA data. The additional power δT_{band}^2 detected by the CBI is significant at the 1.8σ level (BOOMERANG) and the 1.4σ level (MAXIMA), where σ includes calibration uncertainties of 10% (BOOMERANG), 4% (MAXIMA) and 5% (CBI), pointing uncertainties of 11% (BOOMERANG) and 5% (MAXIMA), the

uncertainty of 13% in the δT_{band} measured in the lower l bin (CBI), and an estimated uncertainty of 8% in the δT_{band} measured by BOOMERANG and MAXIMA in the multipole range $300 < l < 700$. It is important to determine whether these differences between the CBI and BOOMERANG-MAXIMA are real. The RING5M experiment (Leitch et al. 2000) reported $\delta T_{\text{band}} = 59^{+8.6}_{-6.5} \mu\text{K}$ at $l \sim 600$, which agrees well with the CBI value and is discrepant at the 1.8σ level with BOOMERANG and at the 1.4σ level with MAXIMA. The CAT values (Scott et al. 1996; Baker et al. 1999) are intermediate between the CBI and BOOMERANG and MAXIMA values, but any differences are significant only at the $\sim 1\sigma$ level.

We have used the likelihoods of our data to explore limits on the cosmological parameters shown in Table 1 for both flat and open model universes with power-law density fluctuation spectra having slope $n = 1$ using CMBFAST (Seljak & Zaldarriaga 1996). Ω is the density parameter, and subscripts “tot,” “b,” “m,” “cdm,” and “ Λ ” refer to the total, baryonic, matter, cold dark matter, and cosmological constant contributions to the density parameter. The ranges and intervals of the parameters are shown in Table 1. For the flat models we find the likelihood peaks at $\Omega_b h^2 = 0.009$ and drops by a factor of 2 at $\Omega_b h^2 = 0.019$ (e.g., Burles & Tytler 1998; O’Meara et al. 2001), and by a factor of 3 at $\Omega_b h^2 = 0.03$. For the open models we have assumed uniform priors for H_0 , $\Omega_b h^2$, Ω_{cdm} , and Ω_{tot} , with Ω_m being uniformly distributed between 0.2 and Ω_{tot} , over the ranges indicated in Table 1, and we find that $\Omega_{\text{tot}} \leq 0.4$ or $\Omega_{\text{tot}} \geq 0.7$ at the 90% confidence level.

We thank Roger Blandford, Marc Kamionkowski, Andrew Lange, and Wallace Sargent for useful comments on this work, Russ Keeney for his tireless efforts on the 40 m telescope, and Angel Otarola for invaluable assistance in setting up the CBI in Chile. We gratefully acknowledge the generous support of Maxine and Ronald Linde, Cecil and Sally Drinkward, and Barbara and Stanley Rawn, Jr., and the strong support of the provost and president of the California Institute of Technology, the PMA division Chairman, the director of the Owens Valley Radio Observatory, and our colleagues in the PMA Division. This work was supported by the National Science Foundation under grants AST 94-13935 and AST 98-02989. We are grateful to CONICYT for granting permission to operate the CBI at the Chajnantor Scientific Preserve in Chile.

TABLE 1
PARAMETER SPACE FOR COSMOLOGICAL LIKELIHOOD ANALYSIS

	Flat Models	Open Models
$\Omega_b h^2$	0.003 \rightarrow 0.03 (0.003)	0.01 \rightarrow 0.03 (0.01)
Ω_{cdm}	0.1 \rightarrow 0.5 (0.04)	$\Omega_m - \Omega_b$
Ω_m	$\Omega_{\text{cdm}} + \Omega_b$	0.2 \rightarrow Ω_{tot} (0.1)
Ω_Λ	$1 - \Omega_m$	$\Omega_{\text{tot}} - \Omega_m$
Ω_{tot}	1	0.2 \rightarrow 1.0 (0.1)
h	0.50 \rightarrow 0.90 (0.04)	0.50 \rightarrow 0.80 (0.05)

The step size for independent variables is shown in parentheses.

REFERENCES

- Baker, J. C., et al. 1999, MNRAS, 308, 1173
Balbi, A., et al. 2000, ApJ, 545, L1
Burles, S. & Tytler, D. 1998, ApJ, 499, 699
Church, S. E., et al. 1997, ApJ, 484, 523
Condon, J. J., Cotton, W. D., Greisen, E. W., Yin, Q. F., Perley, R. A., Taylor, G. B., & Broderick, J. J. 1998, AJ, 115, 169
de Bernardis, P., et al. 2000, Nature, 404, 955
Halverson, N. W., Carlstrom, J. E., Dragovan, M., Holzzapfel, W. L., & Kovac, J., 1998, Proc. SPIE, 3357, 416
Hanany, S., et al. 2000, ApJ, 545, L5
Hobson, M. P., Lasenby, A. N., & Jones, M. E. 1995, MNRAS, 275, 863
Holzapfel, W. L., Carlstrom, J. E., Grego, L., Holder, G., Joy, M., & Reese, E. D. 2000, ApJ, 539, 57
Jaffe, A. H. et al. 2001, preprint (astro-ph/0007333)
Jones, M. E., & Scott, P. F. 1998, in Fundamentals of Cosmology, ed. J. Tran Thanh Van et al. (Gif-sur-Yvette: Eds. Frontieres), 233 (astro-ph/9804175)
Kamionkowski, M., & Kosowsky, A. 1999, Annu. Rev. Nucl. Part. Sci. 49, 77
Lange, A. E., et al. 2001, Phys. Rev. D, 63, 042001
Leitch, E. M., Myers, S. T., Readhead, A. C. S., & Pearson, T. J. 1997, ApJ, 486, L23
Leitch, E. M., Readhead, A. C. S., Pearson, T. J., Myers, S. T., Gulkis, S., & Lawrence, C. R. 2000, ApJ, 532, 37
Mason, B. S., Leitch, E. M., Myers, S. T., Cartwright, J. K., & Readhead, A. C. S. 1999, AJ, 118, 290
Mezger, P. G., Tuffs, R. J., Chini, R., Kreysa, E., & Gemünd, H.-P. 1986, A&A, 167, 145
O'Meara, J.M., Tytler, D., Kirkman, D., Suzuki, N., Lubin, D., Prochaska, J.X., & Wolfe, A.M., 2001, ApJ, in press (astro-ph/0011179)
Padin, S., Cartwright, J.K., Joy, M. and Meitzler, J.C., 2000a, IEEE Trans. Antennas Propagat., 48, 836
Padin, S., Cartwright, J.K., Shepherd, M.C., Yamasaki, J.K. and Holzzapfel, W.L., 2000b, IEEE Trans. Instrum. Meas., (submitted)
Peebles, P.J.E. & Yu, J.T. 1970, ApJ, 162, 815
Readhead, A. C. S., Lawrence, C. R., Myers, S. T., Sargent, W. L. W., Hardebeck, H. E., & Moffet, A. T. 1989, ApJ, 346, 566
Scott, P. F., et al. 1996, ApJ, 461, L1
Seljak, U., & Zaldarriaga, M. 1996, ApJ, 469, 437
Silk, J. 1968, ApJ, 151, 459
Subrahmanyam, R., Kesteven, M. J., Ekers, R. D., Sinclair, M., & Silk, J. 2000, MNRAS, 315, 808
Sunyaev, R. A. & Zeldovich, Ya. B. 1970, Ap&SS, 7, 3
Tegmark, M., Eisenstein, D. J., Hu, W., & de Oliveira-Costa, A. 2000, ApJ, 530, 133
White, M., Carlstrom, J. E., Dragovan, M., & Holzzapfel, W. L. 1999, ApJ, 514, 12
White, R.L., Becker, R.H., Helfand, D.J. & Gregg, M.D. 1997 ApJ, 475, 479
Wrixon, G. T., Welch, W. J., & Thornton, D. D. 1971, ApJ, 169, 171